Ref. Ares(2019)1370979 - 28/02/2019

European Commission

HORIZON 2020
THE FRAMEWORK PROGRAMME FOR RESEARCH AND INNOVATION

Beyond PLANCK

Deliverable 6.3: First Astrophysical Sky Model Products

Authors Kristian Joten Andersen
Hans Kristian Eriksen
Trygve Leithe Svalheim
Harald Thommesen
Ingunn Kathrine Wehus

Date February 28th, 2019

HELSINGIN YLIOPISTO
HELSINGFORS UNIVERSITET
UNIVERSITY OF HELSINKI

planetek hellas

Work Package WP6 - Component separation

Revision History

Version	Authors	Date	Changes
1.0	Kristian Joten Andersen Hans Kristian Eriksen Trygve Leithe Svalheim Harald Thommesen Ingunn Kathrine Wehus	February 28th, 2019	Initial Version

Contents

1 Introduction

Gibbs sampling has been performed with Commander on the latest detector maps from NPIPE in order to acquire the best possible HFI maps for future component separation of the LFI channels. In a feedback loop with NPIPE we have managed to further improve the foreground components maps, giving better residual maps at HFI.

2 First Astrophysical Sky Model Products

The first astrophysical sky model foreground component maps are available for all consortium members at the Oslo "Owl" cluster at: /mn/stornext/d14/bp/first_sky_model_products/

The repository includes the full resolution foreground component maps and band residual maps for both the intensity and polarized sky model. The component maps and chi-squared map for the intensity sky model are shown in Figs. 1-7, while the component maps for the polarized sky model are shown in Figs. 8 and 9.

In order to perform the best possible Gibbs sampling of the LFI channels in the future of BeyondPlanck, one needs the best possible HFI band maps and HFI component maps, as these channels will be freezed, i.e. non changing, in the Gibbs sampling loop over the LFI channels. In collaboration with NPIPE in a feedback loop of detector sky maps from NPIPE and component separation with Commander, the foreground component maps and the HFI band maps have been further improved upon. The addition of new improved HFI single detector maps at higher resolution have been essential for this improvement. The sky maps used to derive the new foreground component maps are the NPIPE version 6v20 sky maps.

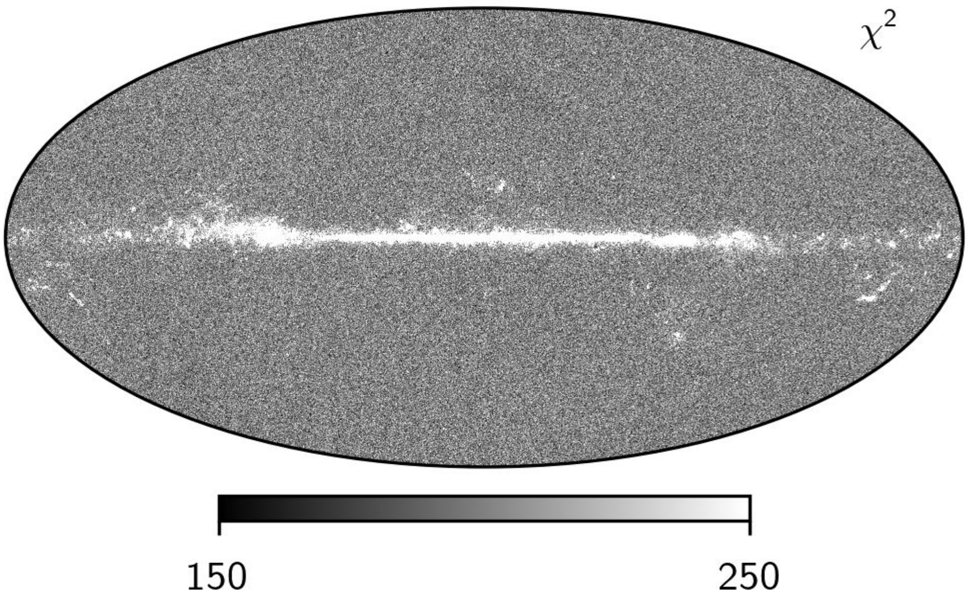

Figure 1. The chi-squared (X^2) map of the full resolution Commander Gibbs sampling of the NPIPE version 6v20 sky maps. The map is plotted with an angular resolution of 5' FWHM. From NPIPE paper (in preparation).

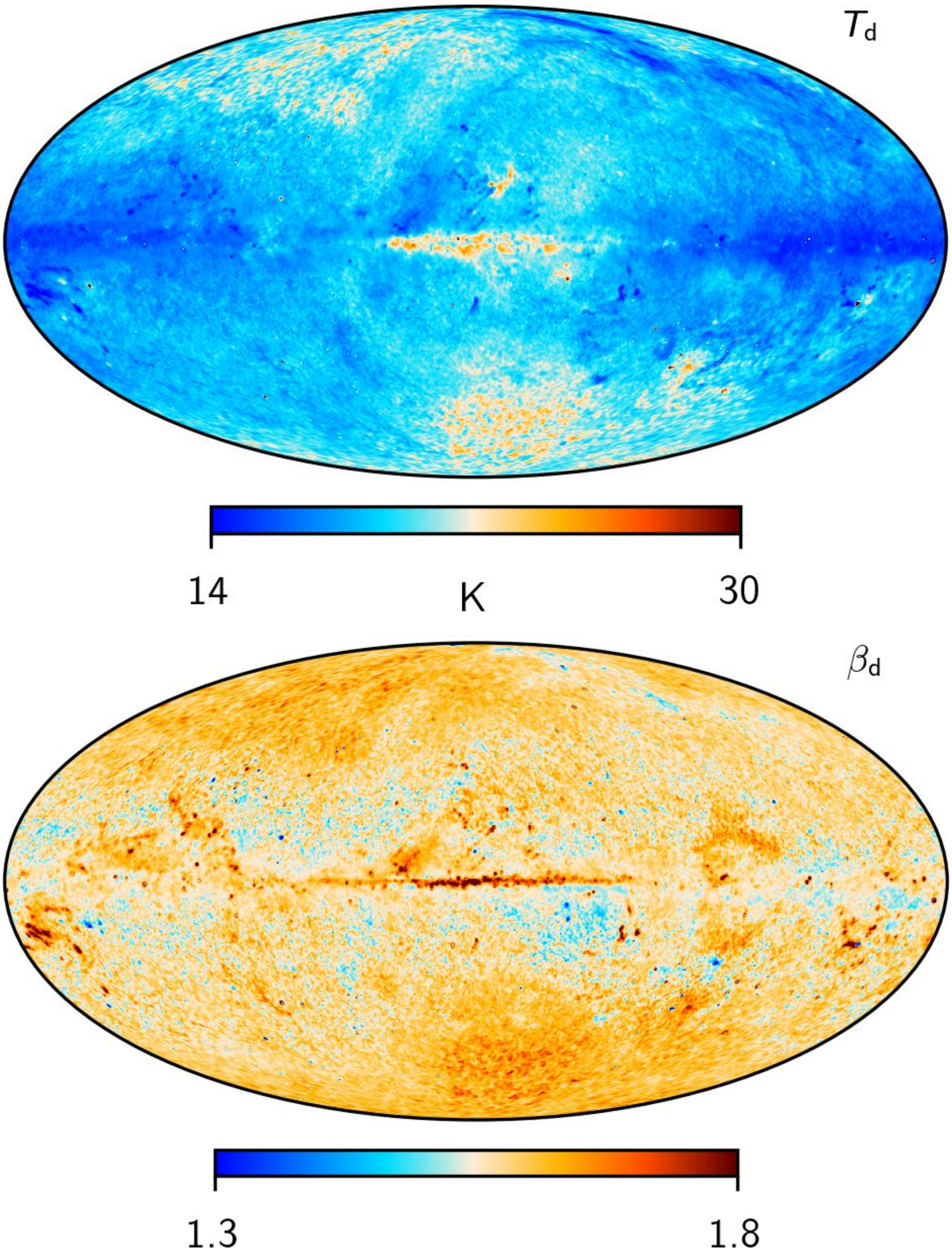

Figure 2. (*Top*) The dust temperature (T_d) map (in kelvins). (*Bottom*) the dust power law coefficient (β_d) map. From the full resolution Commander Gibbs sampling of the NPIPE version 6v20 sky maps. The maps are plotted with an angular resolution of 14’ FWHM. From NPIPE paper (in preparation).

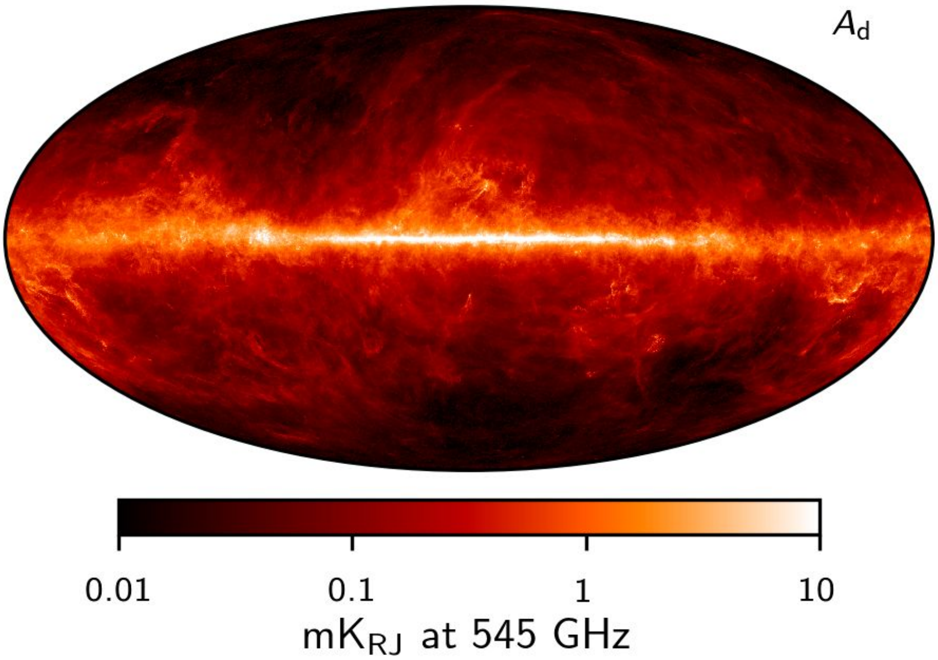

Figure 3. The dust amplitude (A_d) map of the full resolution Commander Gibbs sampling of the NPIPE version 6v20 sky maps. The map is plotted with an angular resolution of 5' FWHM. From NPIPE paper (in preparation).

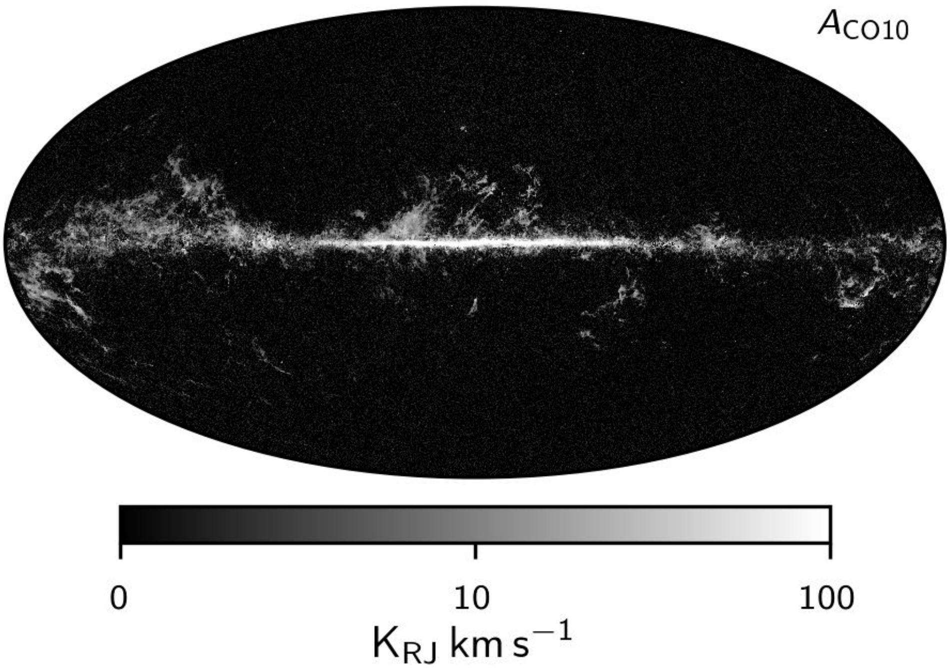

Figure 4. The CO component amplitude (A_{CO10}) map at 100 GHz, i.e. the CO 1→0 line, of the fill resolution Commander Gibbs sampling of the NPIPE version 6v20 sky maps. The map is plotted with an angular resolution of 5' FWHM. From NPIPE paper (in preparation).

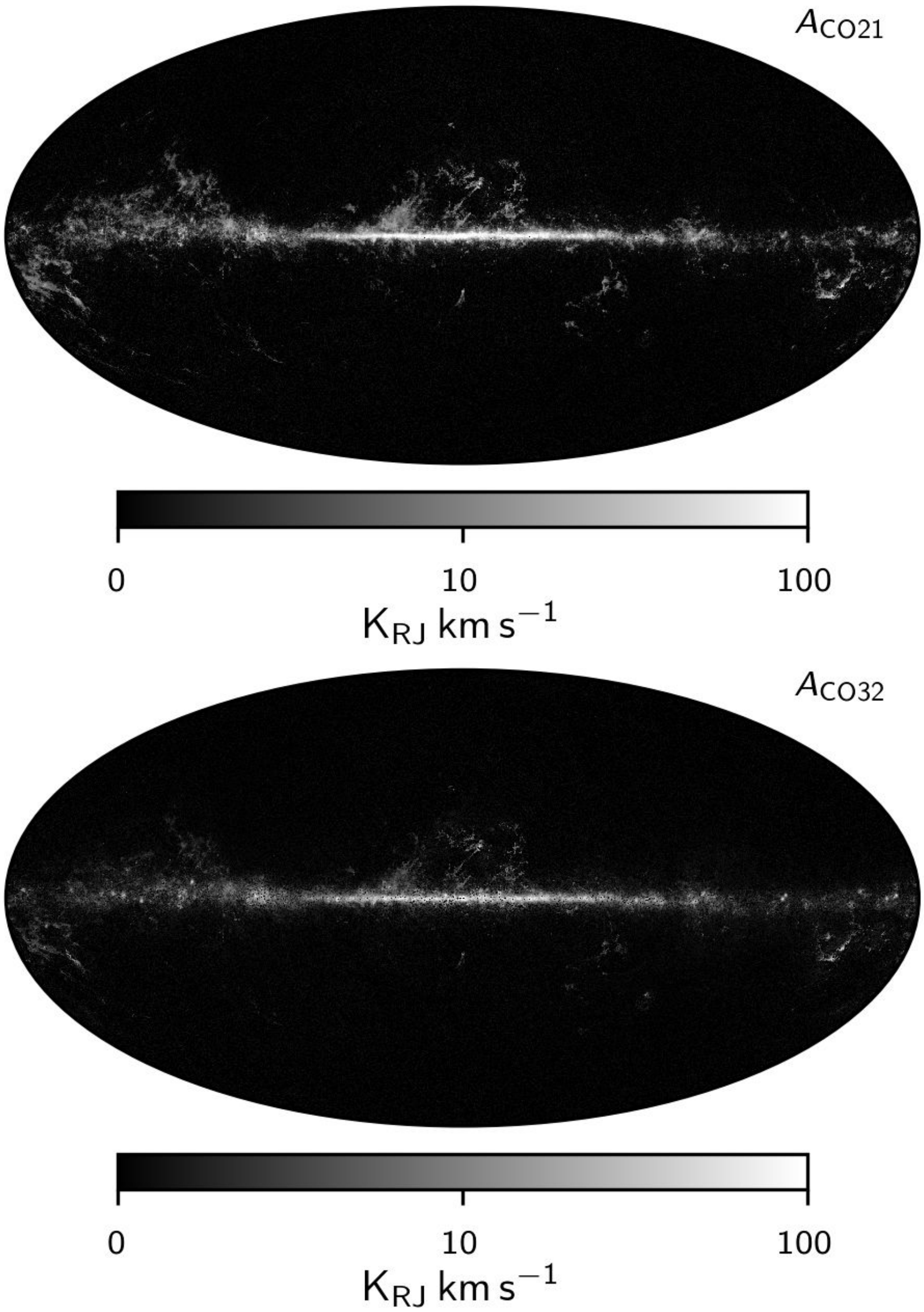

Figure 5. (*Top*) The CO component amplitude map at 217 GHz and (*bottom*) at 353 GHz, respectively the CO 2→1 and CO 3→2 lines, of the full resolution Commander Gibbs sampling of the NPIPE version 6v20 sky maps. The maps are both plotted with an angular resolution of 5' FWHM. From NPIPE paper (in preparation).

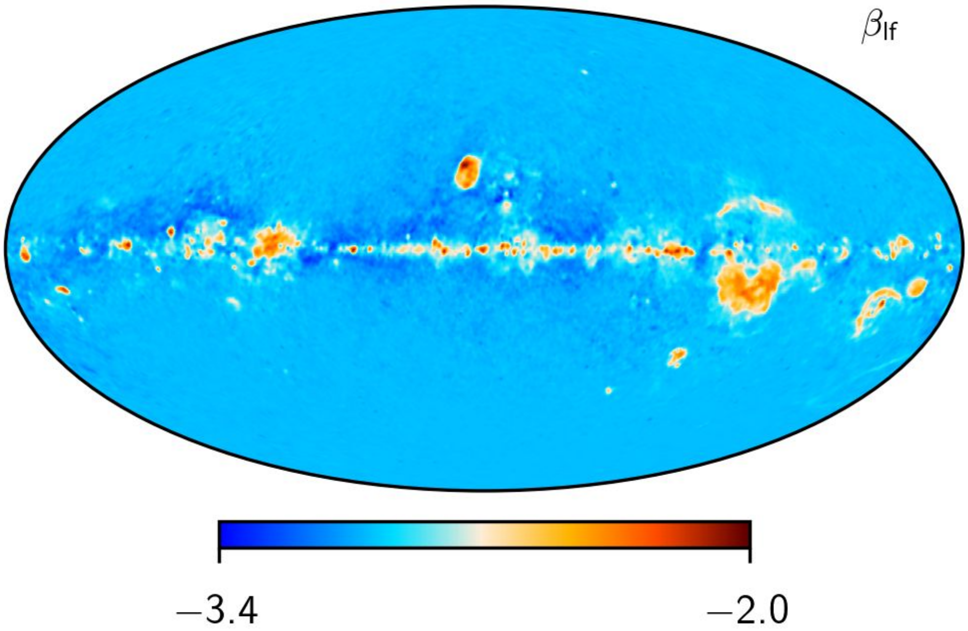

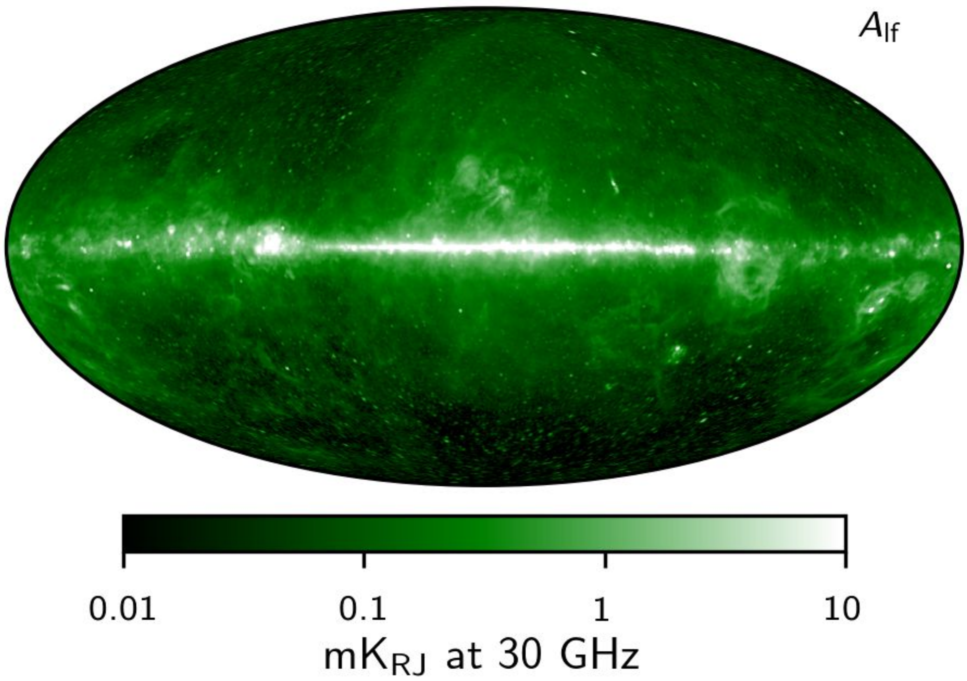

Figure 6. (*Top*) The low frequency component's power law coefficient ($\beta_{\rm lf}$) map and (*bottom*) the low frequency component amplitude ($A_{\rm lf}$) map of the full resolution Commander Gibbs sampling of the NPIPE version 6v20 sky maps. The maps are plotted with an angular resolution of 60' and 40' FWHM respectively. From NPIPE paper (in preparation).

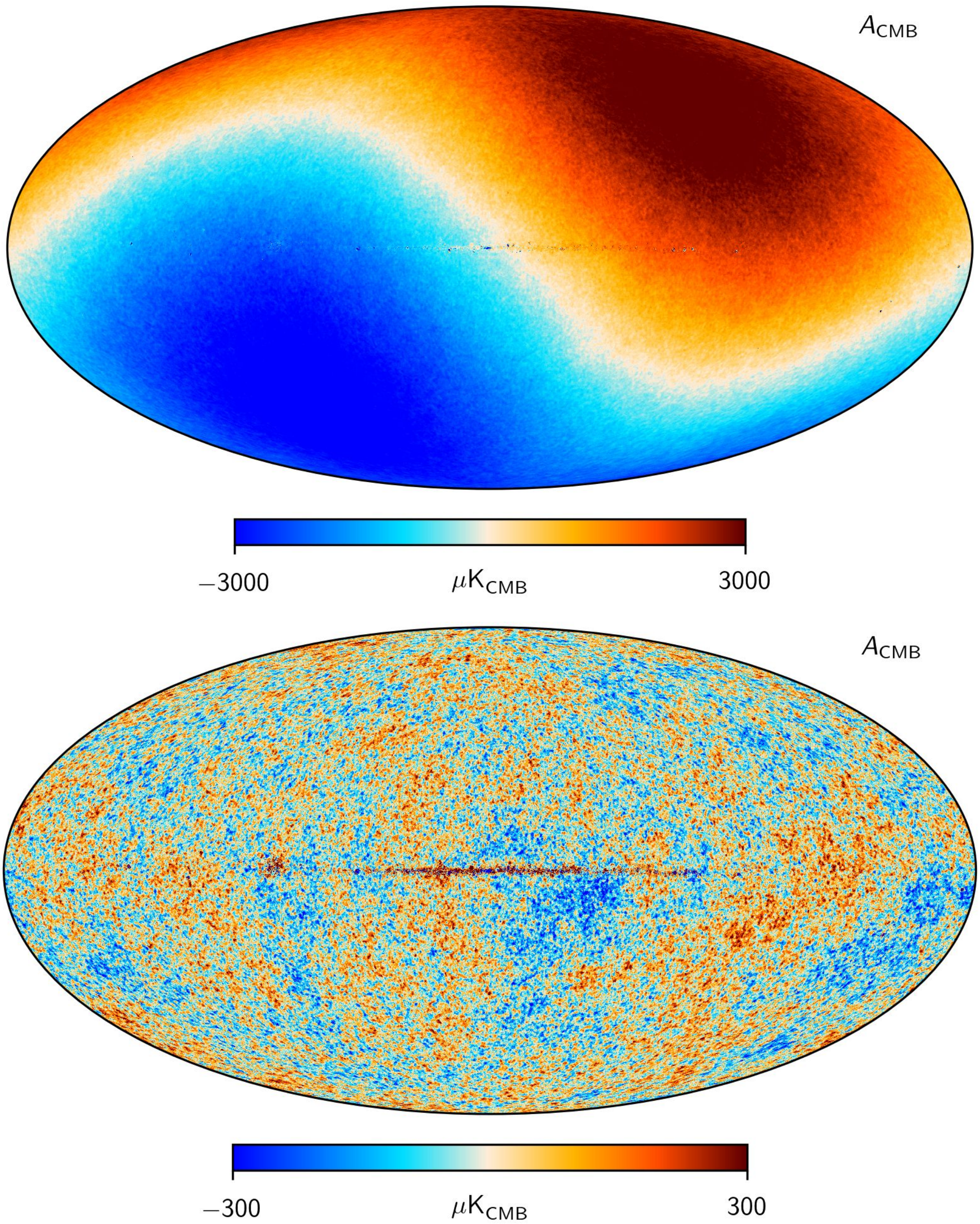

Figure 7. The plots show the CMB fluctuations of the full resolution Commander Gibbs sampling of the NPIPE version 6v20 sky maps. In the bottom plot the CMB dipole has been subtracted. The maps are plotted with an angular resolution of 5’ FWHM. From NPIPE paper (in preparation).

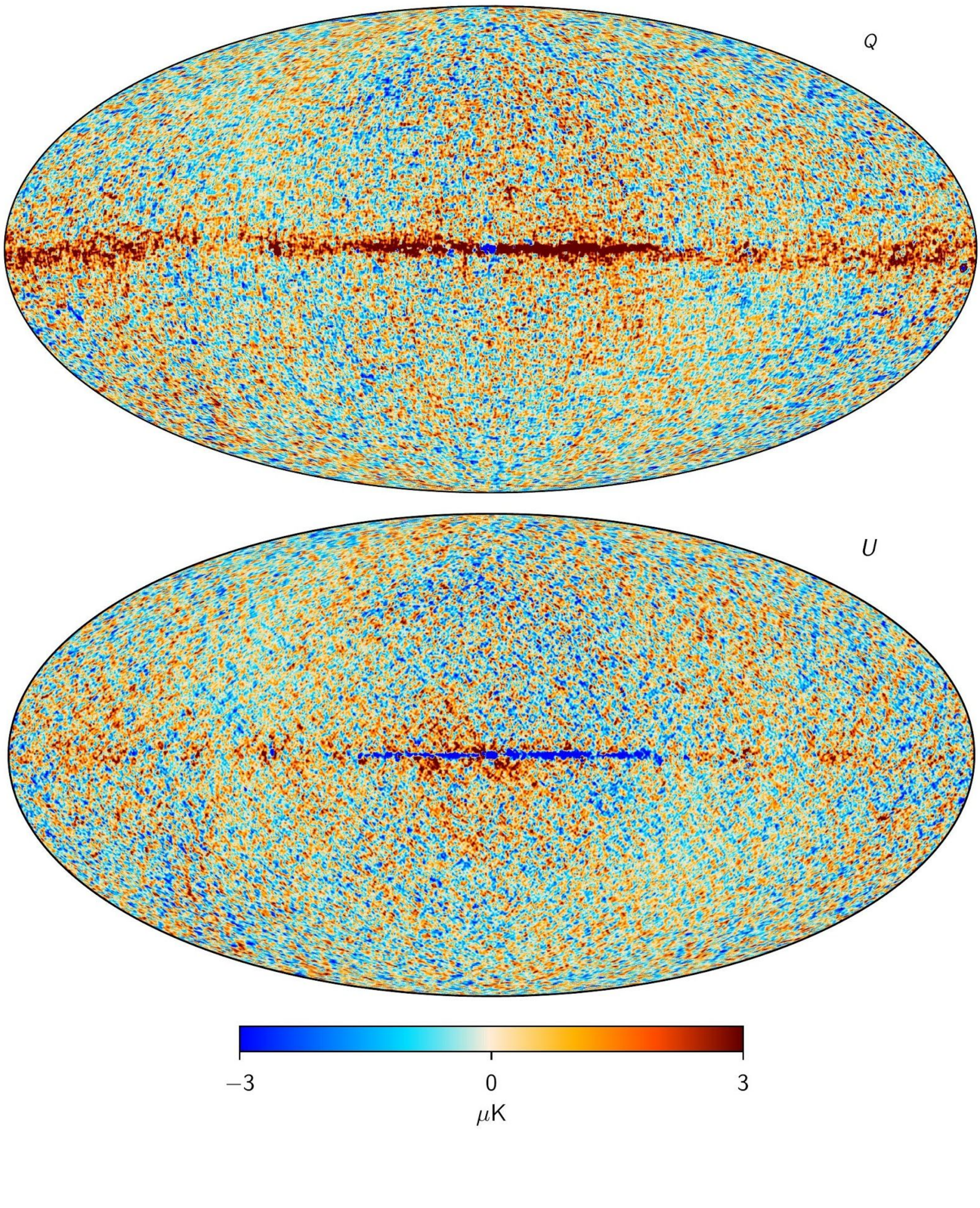

Figure 8. CMB polarization maps derived from the NPIPE 6v20 data set. Top and bottom panels show Stokes *Q* and *U* parameters, respectively, both plotted with an angular resolution of 40' FWHM. From NPIPE paper (in preparation).

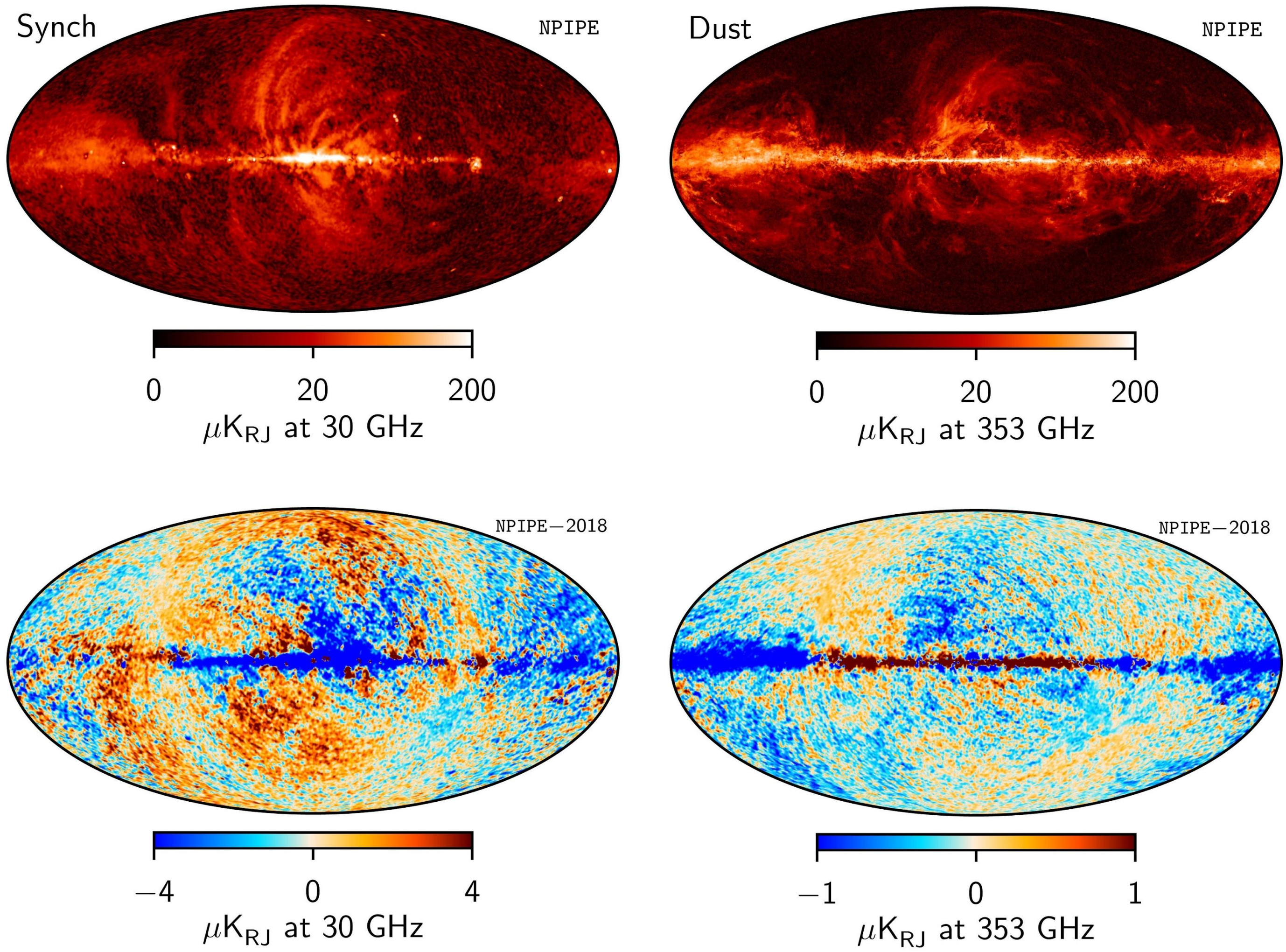

Figure 9. (*Top*:) Synchrotron (*left*) and thermal dust (*right*) polarization amplitude ($P = (Q^2 + U^2)^{1/2}$) maps derived from the NPIPE 6v20 data set. The synchrotron map is smoothed to an angular resolution of 40’ FWHM, and the thermal dust map is smoothed to angular resolution of 5’ FWHM. (*Bottom*:) Corresponding polarization amplitude difference maps taken between the NPIPE and the Planck 2018 component maps. Both maps are smoothed to a common resolution of 60’ FWHM. Note that the top panels employ the non-linear Planck colour scale, while the bottom panels employ linear colour scales. From NPIPE paper (in preparation).

2.1 Tasks Performed

The following tasks have been performed on the sky maps from NPIPE:

- Commander 1: Low resolution Gibb's sampling for band gain and bandpass correction, CO line ratio estimation and creation of new low resolution component maps.
- Commander 2: Full resolution Gibb's sampling with input component maps and instrumentation parameters from Commander 1. Output of new high resolution component maps.
- Feedback of the new component maps to NPIPE for further improvement of the detector sky maps.

2.2 Intensity comparison to Planck 2015 and initial sky model

As mentioned earlier in section 2 one wants the best possible HFI sky maps to initiate the Gibb's sampling of the LFI channels. Until now the Planck 2015 results (see Planck Collaboration 2015) are the best model for the foreground components and would have been the initialization maps of the HFI channels if we did not have better maps. By comparing the new maps to the Planck 2015 results (and to our initial sky model) one can see a clear improvement in the residual maps for many detectors. Figures 10 and 11 show the residual maps of four detectors of the Planck 2015 results, the initial sky model (NPIPE version 5v21) and the most recent sky model derived from Gibbs sampling of the NPIPE version 6v20 sky maps.

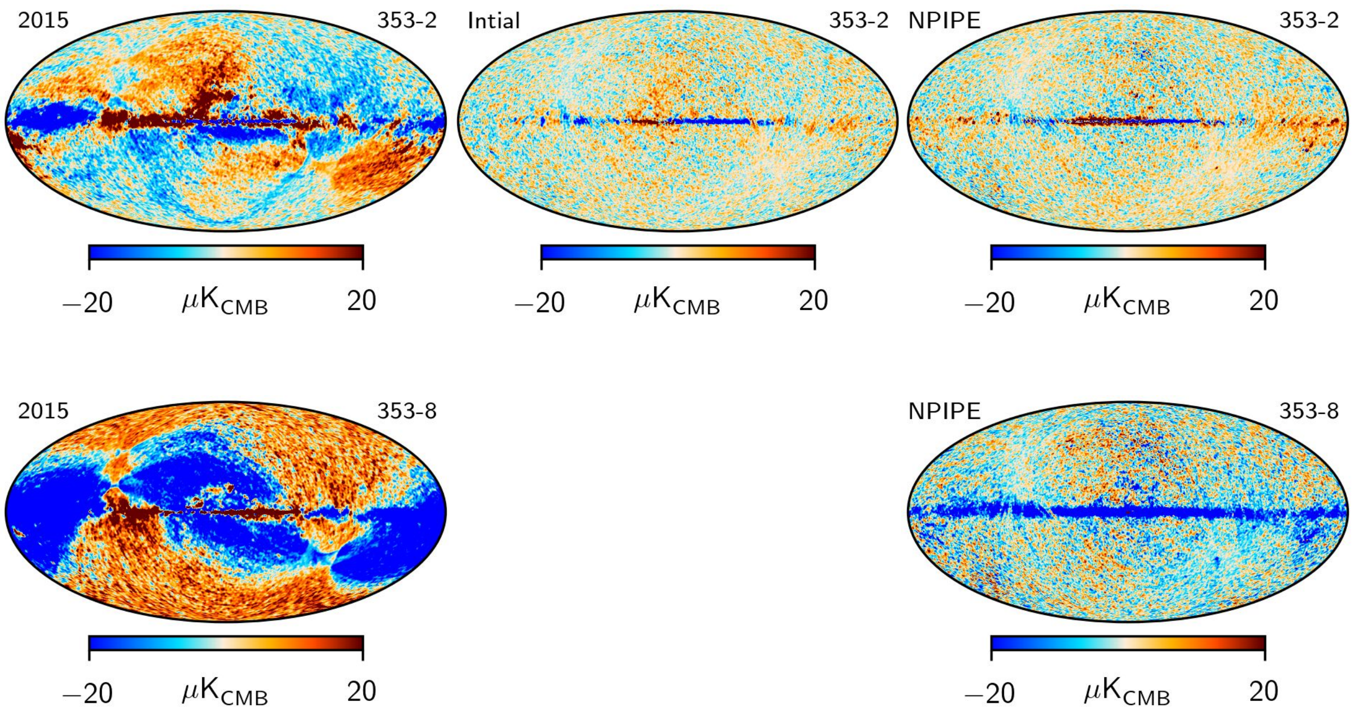

Figure 10. The figure shows the residual maps of detectors nr. 2 and 8 at 353 GHz for the Planck 2015 results (*left*), the initial sky model in collaboration with NPIPE (*middle)* and the new sky model in collaboration with NPIPE (*right*). The initial sky model did not include the 353-8 detector map and is therefore empty. The maps are all smoothed to a common angular resolution of 1° FWHM. From NPIPE paper (in preparation).

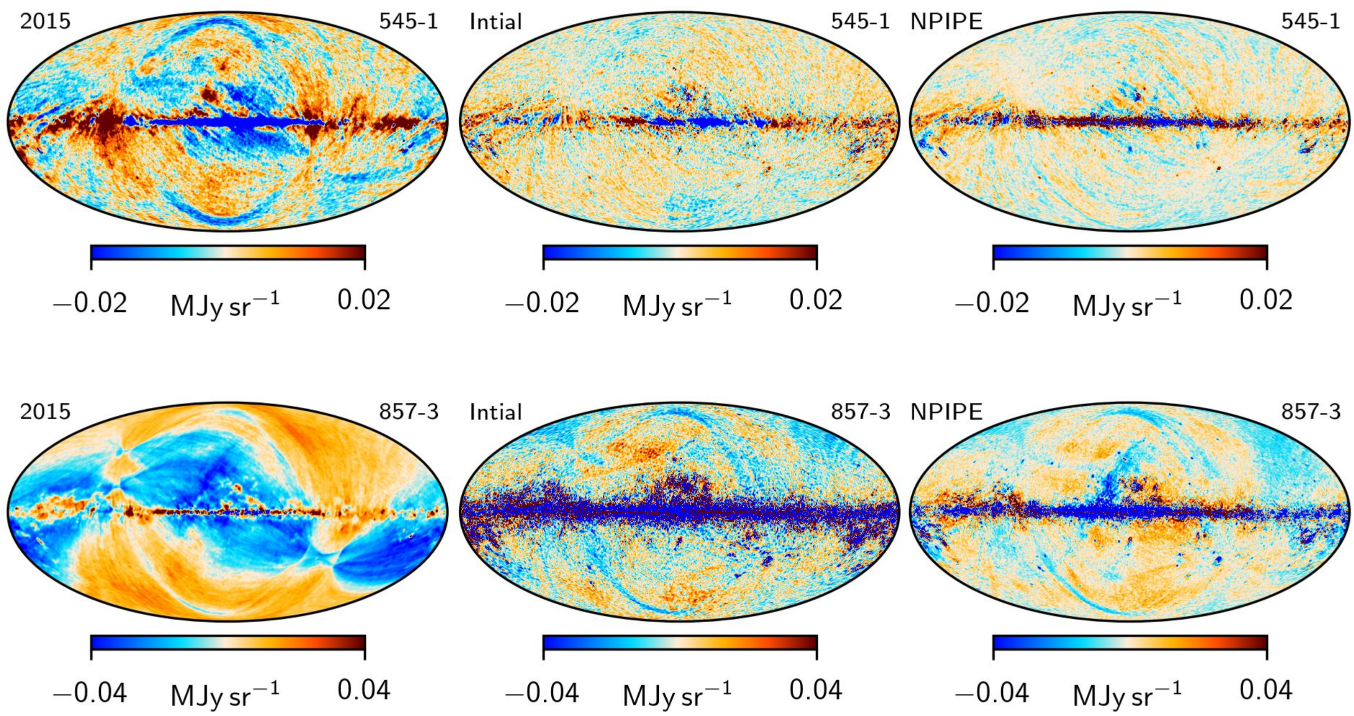

Figure 11. The figure shows the residual maps of detector nr. 1 at 545 GHz and detector nr. 3 at 857 Ghz for the Planck 2015 results (*left*) and the most recent sky model in collaboration with NPIPE (*right*). The maps are all smoothed to a common angular resolution of 1° FWHM. From NPIPE paper (in preparation).

While the Planck 2015 single detector sky maps have a HEALPix resolution parameter of N_{side} = 256, and the Planck 2018 only have one (all-bands) map per frequency at a resolution of N_{side} = 1024 for LFI and N_{side} = 2048 for HFI, the NPIPE version 6v20 has sky maps for all single detectors sharing the same resolution as Planck 2018, except for 217-857 GHz where the resolution of the single detectors are N_{side} = 4096. The improved resolution to N_{side} = 4096 has helped removing ringing effects around bright point sources, and are now more dominated by asymmetrical beams. Figure 12 shows plots of the CMB around Tau A for both the initial sky model (NPIPE 5v21) and the most recent sky model (NPIPE 6v20). From NPIPE paper (in preparation).

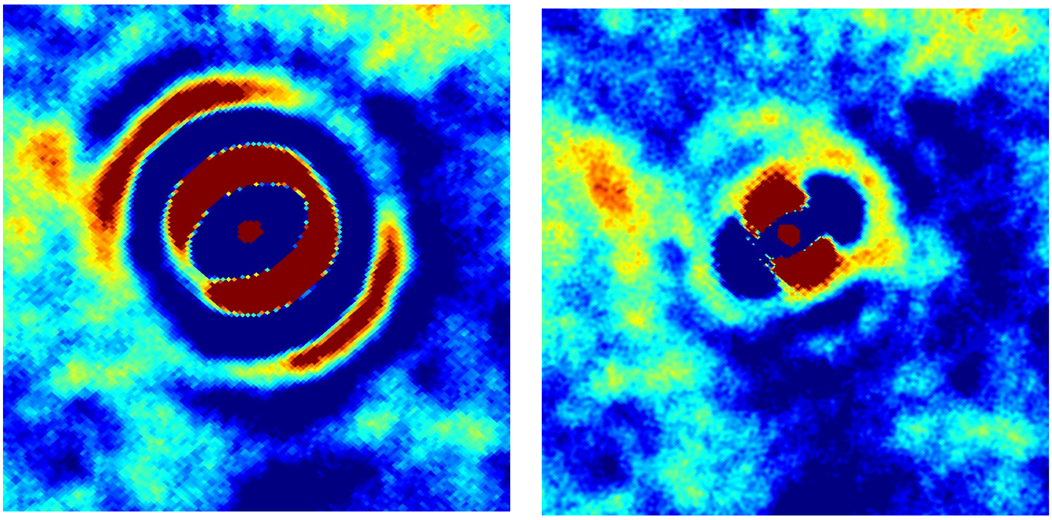

Figure 12. The figure shows a 4°x4° zoom-in of the CMB around Tau A, centered around Galactic coordinates (*l*, *b*) = (184.5°, -6.0°). (*Left*) From the component separation of NPIPE 5v21 sky maps. (*Right*) From the component separation of NPIPE 6v20 sky maps. The maps are plotted with an angular resolution of 5' FWHM, on a color range from -300 (blue) to +300 (red) micro kelvins. The ringing effect is cleary visible in the results from the NPIPE 5v21 sky maps, while in the model from the NPIPE 6v20 sky maps have no ringing but a problem with asymmetrical beams.

2.3 Polarization comparison to Planck 2015 & Planck 2018

In Figure 13 we see a comparison of the large-scale Commander CMB polarization maps as derived from the Planck 2015 (top), 2018 (middle) and NPIPE (bottom) data sets. The amount of large-scale residuals decrease significantly from data set to data set.

Corresponding large angular scale power spectra plot derived from data half-splits are shown in Figure 14. The improved systematics control is clearly evident in the form of a lower bias at large scales.

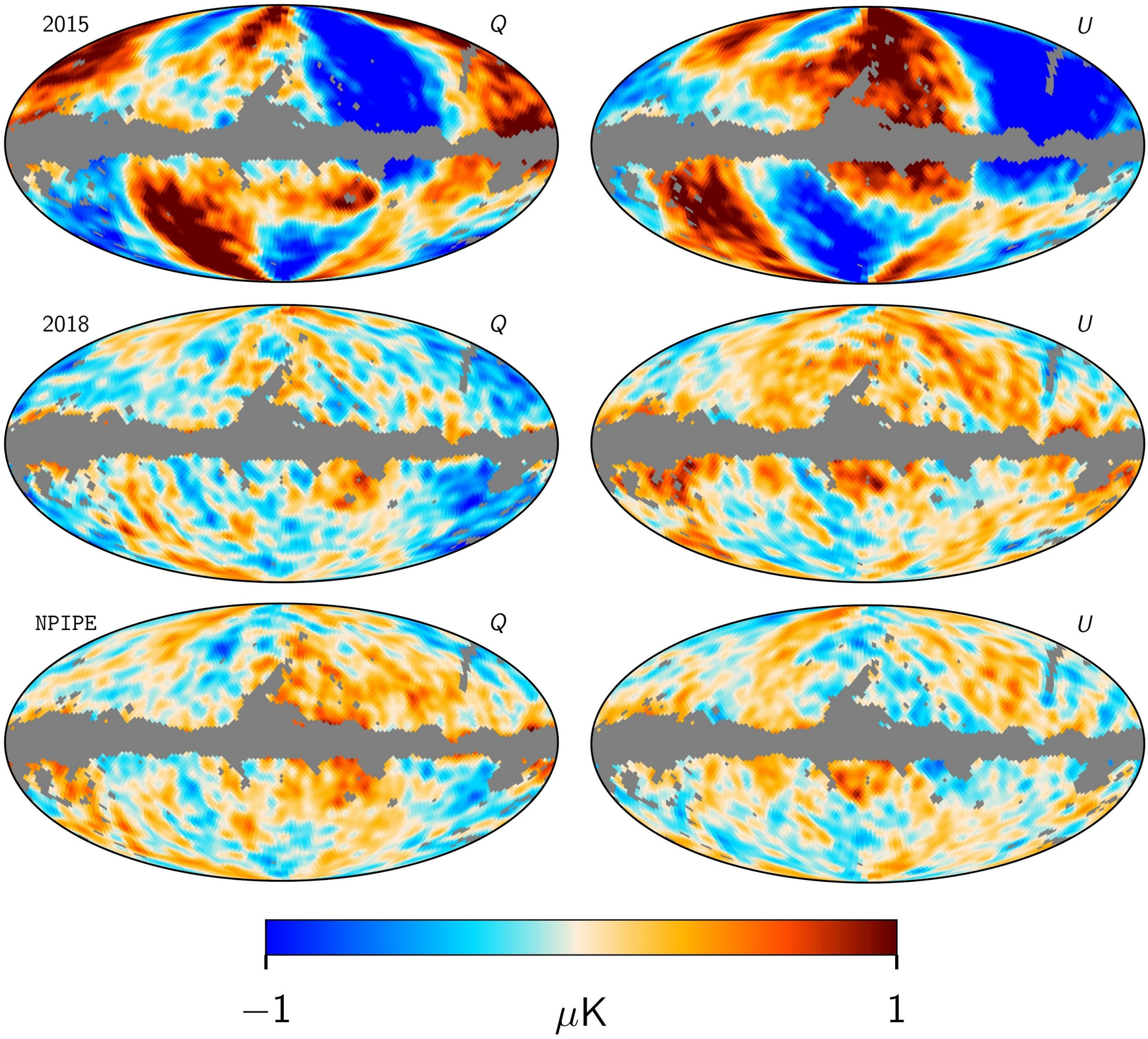

Figure 13. Comparison of large-scale Commander CMB polarization maps derived from the Planck 2015 (*top row*), the Planck 2018 (*middle row)*, and the NPIPE (*bottom row*) data releases. Note that the large-scale Planck 2015 CMB map was never publicly released, due to the large amount of residual systematic effects. The left and right columns shows Stokes *Q* and *U* parameters, respectively, and the gray region corresponds to the Planck 2018 common component separation mask (Planck Collaboration IV 2018). From NPIPE paper (in preparation).

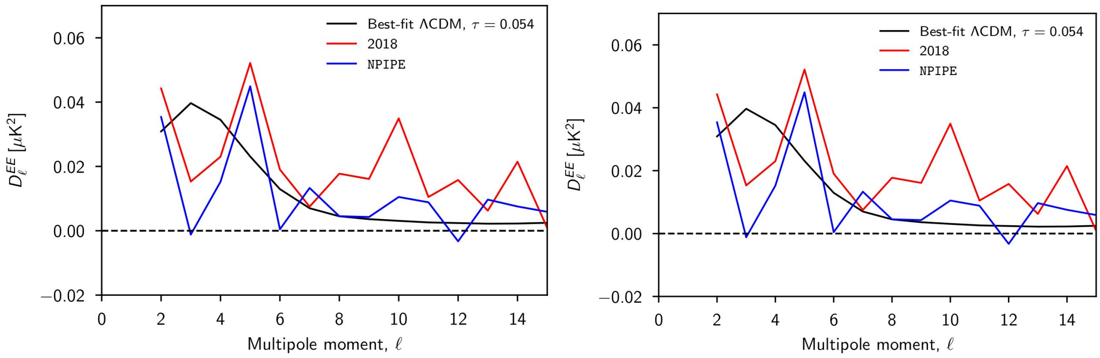

Figure 14. Angular CMB polarization cross-power spectra evaluated from the Planck 2018 (red curves) and NPIPE (blue curves) data sets, zoomed in on large angular scales. EE and BB spectra are shown in the left and right panels, respectively. The Planck 2018 best-fit ΛCDM EE spectrum is plotted with a black solid line. The cross-spectra are evaluated from the most independent data split that is available for each data set, corresponding to the A/B detector split for NPIPE and the half-mission split for the Planck 2018 data set. Corrections for the low-` 143A×143B transfer function have been applied to both sets. From NPIPE paper (in preparation).

2.4 The CMB dipole

Starting with the NPIPE and BeyondPlanck data release, all Planck detector and frequency maps will be delivered with the CMB solar dipole still present. This allows for joint absolute calibration and component separation, and thereby eliminates important degeneracies in the derived models.

We have implemented a new Wiener filter based dipole estimator, and applied this to the most recent data set. The results from these calculations are shown in Table 1 and Figure 15. In addition to provide a more robust estimate of the central values for the various parameters, this approach also provides more meaningful estimates of the uncertainties. We see in particular that the official Planck HFI uncertainties are clearly internally inconsistent, given the large changes from data release to release. In contrast, our uncertainties are numerically larger than the HFI ones, but at the same time we believe the true uncertainties are in fact smaller, due to the improved estimator.

Table 1: Comparison of Solar dipole measurements from COBE, WMAP, and Planck. From NPIPE paper (in preparation).

Experiment	Amplitude [μK_{CMB}]	Galactic coordinates l [deg]	Galactic coordinates b [deg]	Reference
COBE [a,b]	3358 ± 23	264.31 ± 0.16	48.05 ± 0.09	Lineweaver et al. (1996)
WMAP [c]	3355 ± 8	263.99 ± 0.14	48.26 ± 0.03	Hinshaw et al. (2009)
LFI 2015 [b]	3365.5 ± 3.0	264.01 ± 0.05	48.26 ± 0.02	Planck Collaboration II (2016)
HFI 2015 [d]	3364.29 ± 1.1	263.914 ± 0.013	48.265 ± 0.002	Planck Collaboration VIII (2016)
LFI 2018 [b]	3364.4 ± 3.1	263.998 ± 0.051	48.265 ± 0.015	Planck Collaboration II (2018)
HFI 2018 [d]	3362.08 ± 0.99	264.021 ± 0.011	48.253 ± 0.005	Planck Collaboration III (2018)
NPIPE [a,c]	**3366.6 ± 1.0**	**263.986 ± 0.035**	**48.247 ± 0.023**	

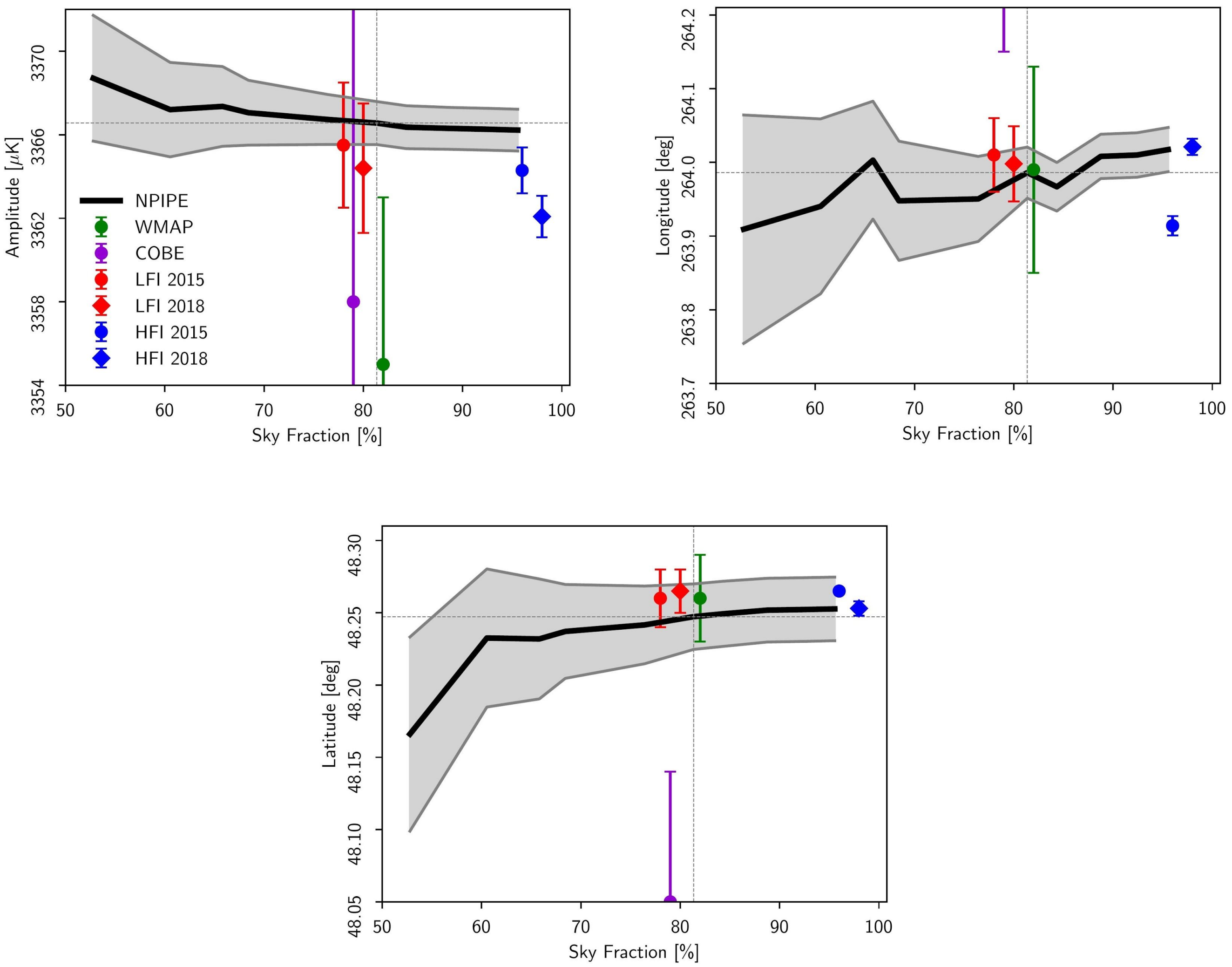

Figure 15. CMB solar dipole parameters as a function of sky fraction as estimated from NPIPE data. The solid black lines show the posterior mean derived with a Wiener filter estimator, and the gray bands show corresponding ±1σ confidence regions including both statistical and systematic uncertainties. The three panels show (*top left*) amplitude, (*top right*) longitude and (*bottom*) latitude parameters. For comparison, estimates from COBE, WMAP, and Planck LFI and HFI are shown as individual coloured data points. The dotted lines represent the NPIPE values that are adopted as final optimal estimates, and summarized in Table 1, defined by a sky fraction of f_{sky} = 0.81. From NPIPE paper (in preparation).

2.5 Future improvements

With the inclusion of single detector channels at the HFI frequencies, Commander2 has shown problems correcting for radio sources as the memory usage has grown beyond the Owl cluster's capacity. This is likely a bug in the code that will be examined. Until this bug is fixed, all full resolution Gibbs sampling with Commander 2 is not correcting for radio sources, which are showing as bright sources in the CMB maps or the other component maps.

In addition to radio sources, we are working on implementing additional CO components through the Carbon-13 isotope, which has a slightly different line emission frequency, and the CO gas' radial velocity through the GAIA survey, which is affecting the true frequency of the line emission. Preliminary results on the C-13 isotope looks promising, while the implementation of the CO gas' radial velocity is still a work in progress. In addition to this, the application of the external CO survey, Dame et. al. as a reference map will allow us to solidify the CO 1-0 component, resulting in more robust sampling of line ratios. This will in turn allow us to better sample other component parameters.

Furthermore, with the inclusion of additional external data sets in the low-frequency regime, we gain the ability to disentangle degenerate foregrounds. By including the 408 MHz Haslam et al. survey, we get a powerful probe of synchrotron emission, which we, with the assistance of the WMAP data in the range of 23 to 94 GHz, use to sample free-free and AME emission independently, as opposed to a joint low-frequency component.

Finally, once the BeyondPlanck pipeline starts to provide LFI sky maps we will start using these maps for the LFI frequency bands instead of the NPIPE maps, and so get the whole pipeline running.

3 References

Hinshaw, G., Weiland, J. L., Hill, R. S., et al., Five-Year Wilkinson Microwave Anisotropy Probe (WMAP) Observations: Data Processing, Sky Maps, and Basic Results. 2009, ApJS, 180, 225, arXiv:0803.0732

Lineweaver, C. H., Tenorio, L., Smoot, G. F., et al., The Dipole Observed in the COBE DMR 4 Year Data. 1996, ApJ, 470, 38, arXiv:astro-ph/9601151

Planck Collaboration II, Planck 2015 results. II. Low Frequency Instrument data processing. 2016, A&A, 594, A2, arXiv:1502.01583

Planck Collaboration VIII, Planck 2015 results. VIII. High Frequency Instrument data processing: Calibration and maps. 2016, A&A, 594, A8, arXiv:1502.01587

Planck Collaboration X, Planck 2015 results. X. Diffuse component separation: Foreground maps. 2016, A&A, 594, A10, arXiv:1502.01588

Planck Collaboration II, Planck 2018 results. II. Low Frequency Instrument data processing. 2018, A&A, submitted, arXiv:1807.06206

Planck Collaboration III, Planck 2018 results. III. High Frequency Instrument data processing. 2018, A&A, accepted, arXiv:1807.06207

Planck Collaboration IV, Planck 2018 results. IV. Diffuse component separation. 2018, A&A, submitted, arXiv:1807.06208

Planck Collaboration, NPIPE – joint Planck LFI and HFI data processing, 2019, in preparation.